

Computational tools for the determination of factor of safety and location of the critical circular failure surface for slopes in Mohr-Coulomb dry ground

C. Carranza-Torres^{1*} & E. Hormazabal²

¹*Department of Civil Engineering, University of Minnesota, Duluth Campus, Minnesota, USA*

²*SRK Consulting Chile, Santiago, Chile*

*carranza@d.umn.edu (corresponding author's E-mail)

Abstract

This paper presents computational tools for the quick estimation of factor of safety and location of the critical circular failure surface for simple slope problems. The analysis presented here applies to slopes of arbitrary height and inclination angle excavated in homogeneous/isotropic dry ground, assumed to obey the Mohr-Coulomb shear failure criterion, and characterized by arbitrary values of unit weight, cohesion and internal friction angle. The proposed procedure is based on ideas originally laid out in the classical book *Rock Slope Engineering* by Hoek and Bray (1981) and more recently in the books by Read and Stacey (*Guidelines for Open Pit Slope Design*) and by Wyllie (*Rock Slope Engineering, Civil Applications*) from 2009 and 2018, respectively. Development of the proposed procedure involved computation of approximately 3,400 selected cases of slopes using the Bishop Method in the limit equilibrium software SLIDE by Rocscience. Results obtained from the analysis are summarized in dimensionless graphical representations that not only allow factors of safety and location of the critical circular failure surface to be estimated, but also important, to put light into the fundamental problem of establishing the concept of mechanical similarity of slopes excavated in Mohr-Coulomb ground with regard to factors of safety and position of the critical circular failure surface. In addition to the graphical representation of factor of safety, the paper also provides an equation to compute the factor of safety of slopes based on these representations. Considering that in the current practice of geotechnical engineering design the use of computer spreadsheets may be preferred over the use of dimensionless charts, the proposed procedure is implemented in a simple to use EXCEL workbook that is freely available to readers, and that allows determination of factor of safety and location of the failure surface, as it would be obtained with the Bishop Method in the limit equilibrium method software SLIDE. Finally, to illustrate the application of the proposed tools, a practical example involving the analysis of stability of a slope in an actual open pit mine is provided.

Keywords: Slope stability, Limit equilibrium, Method of slices, Bishop method, Factor of safety, Mohr-Coulomb.

1 Introduction

Computation of factor of safety against failure and location of the critical failure surface forms the basis of the current practice of stability analysis of slopes in civil and mining engineering, whether carried out in a deterministic or in a probabilistic manner (see, for example, Vanmarcke 1980; Juang et al. 1998; Steffen et al. 2008). This is particularly true for slopes in soils or in weak rocks, or for slopes in highly jointed rock masses, for which the assumption of material continuity and isotropy can be regarded as valid (Read & Stacey 2009; Wyllie 2018). For the case of slopes in soil and rock (to be referred indistinctly using the term *ground* in the remainder of this paper), when the ground is relatively homogeneous and isotropic, it is common practice to assume that the critical failure surface has a circular shape (see, for example, Abramson et al. 2002; Duncan et al. 2014).

The Mohr-Coulomb shear failure criterion, characterized by internal friction angle and cohesion parameters, is perhaps the simplest material model that can be used to carry out a slope stability analysis (see, for example, Coduto et al. 2011; Verruijt 2012). Although the Mohr-Coulomb shear strength model is extensively used in slopes stability analyses in homogeneous/isotropic soils, the Hoek-Brown failure shear failure criterion is the material model that is generally preferred in slope stability analyses in (assumed homogeneous/isotropic) rock masses (Hoek & Brown 1980; Hoek & Brown 1997). Conveniently, it is always possible, to compute equivalent Mohr-Coulomb frictional parameters from Hoek-Brown parameters for the characteristic range of stresses in the problem to be analyzed (Hoek et al. 2002).

There exists various methods for computing the factor of safety and location of the critical circular failure surface for a slope. Among them, *limit equilibrium* methods, *limit analysis* methods and *full numerical* methods (Potts & Zdravkovic 1999). The so-called *strength reduction technique*, normally implemented in *finite element* or *finite difference* software, is another method for computing the stability of a slope that has gained popularity in recent years (see, for example, Matsui & San 1992; Dawson et al. 1999; Griffiths & Lane 1999; Hammah et al. 2007). All these existing methods of analysis require use of computer software for their implementation, as they are compute-intensive. With this regard, it is remarkable that in contrast with other problems in geotechnical engineering, there are no rigorous analytical closed-form equations available for computing the factor of safety and position of the critical circular failure surface for slopes of arbitrary inclination angle, even for the simplest case of a ground that obeys the Mohr-Coulomb shear failure criterion.

Despite of its introduction middle of the last century, the *method of slices*, which is a particular formulation of the limit equilibrium method, is still the most popular method to estimate the factor of safety and location of the critical failure surface for slopes (see, for example, Abramson et al. 2002; Duncan et al. 2014). Within the method of slices, there exist various formulations, including the Bishop, Janbu, Spencer and Morgenstern-Price methods (see Bishop 1955; Janbu 1954b, 1954a; Spencer 1967; Morgenstern & Price 1965, respectively). The Bishop method is a popular one since it tends to give similar results (i.e., factors of safety and location of the failure surface) as those obtained with more elaborated methods (e.g., the Spencer and Morgenstern-Price methods) with less computer effort (Abramson et al. 2002). Implementation of the Bishop method of slices to compute factor of safety and location of the critical circular failure surface for a slope requires use of specialized computer software. There exist various commercial packages of this type, for example GEO5 (Fine Inc. 2016), SLIDE (Rocscience Inc. 2015), SLOPE/W (Geo-Slope Inc. 2012), XSTABL (Interactive Software Designs Inc. 2007).

Considering the fact that there are no closed-form solution or that compute-intensive methods are required for the determination of factor of safety and location of critical failure surface for slopes in Mohr-Coulomb frictional ground, many authors have proposed *dimensionless charts* as a means of summarizing and conveying the results of slope stability analyses (e.g., obtained from application limit equilibrium methods) in a format that can be readily used in practice (see, for example, Taylor 1948; Bishop & Morgenstern 1960; Spencer 1967; O'Connor & Mitchell 1977; Cousins 1978; Hoek & Bray 1981; Michalowski 2002; Baker 2003; Steward et al. 2010). It also has to be mentioned that other authors have gone a further step and have combined existing or new dimensionless charts with observations of actual slope stability cases in the field, to produce *empirical* dimensionless (stability) charts (see, for example, Haines et al. 1991; Sjoberg 2000; Kotze & Bosman 2015).

Among the various proposed dimensionless stability charts for slopes in Mohr-Coulomb ground obtained from limit equilibrium models, the ones presented in the classical book by Hoek & Bray (1981), and more recently included in the books by Read & Stacey (2009) and Wyllie (2018), deserve particular attention. These stability charts use a particular form of dimensionless scaling originally proposed by Bell (1966) that allows a compact (perhaps the most compact) representation of factor of safety for slopes of planar face of arbitrary inclination angle and height, in a ground of arbitrary values of unit weight, internal friction angle and cohesion. Although not explicitly mentioned in the book, the repre-

sentation proposed by Hoek & Bray (1981) forms the basis for establishing a concept of mechanical similarity of factor of safety for slopes in Mohr-Coulomb ground.

This paper builds on and extends the dimensionless representations proposed by Hoek & Bray (1981) for the case of slopes in Mohr-Coulomb *dry* ground. In addition to re-casting the dimensionless representation of factor of safety to be able to provide a (best fit) closed-form equation to compute factor of safety for slopes, the paper expands on the analysis by Hoek & Bray (1981) by providing dimensionless representations that allow to define the location of the critical circular failure surface, as obtained with the Bishop method of slices with the software SLIDE (Rocscience Inc. 2015). These proposed dimensionless representations allow the concept of mechanical similarity of factor of safety and location of the critical circular failure surface of slopes in Mohr-Coulomb ground to be established.

Considering that in modern geotechnical engineering practice computer spreadsheets or simple equations are preferred over graphical dimensionless representations, this paper also presents a computer EXCEL (Microsoft 2016) worksheet that summarizes the results of the proposed dimensionless stability graphical representations and that can be conveniently used to quickly determine factors of safety and position of critical circular failure surfaces.

2 Problem statement

The problem considered in this study is shown in Figure 1. A slope of inclination angle α , and height H , is excavated in an assumed homogeneous/isotropic *dry* ground of unit weight γ , that obeys the Mohr-Coulomb shear failure criterion, and that is characterized by a cohesion c and an internal friction angle ϕ . The origin of a system of cartesian coordinates (x,y) is assumed to be located at the *toe* of the slope (point O in Figure 1). When the strength of the ground is affected by the factor of safety, the slope is assumed to be in a limit state of equilibrium with a critical *circular* failure surface of radius R and a center of coordinates x_C and y_C (point C in Figure 1). The *starting* point of the failure surface (point A in the figure) has coordinates x_A and y_A , while the *ending* point of the failure surface (point B in the figure) has coordinates x_B and y_B . To simplify the problem, no explicit tension crack is considered at the ending point of the failure surface.

According to the *method of slices* of slope stability analysis, when failure of the slope occurs at the critical circular failure indicated in Figure 1, the shear strength of the ground is fully mobilized on the failure surface (see, for example, Coduto et al. 2011; Verruijt 2012). For the case of the Mohr-Coulomb shear failure criterion considered in this study, this condition is written as follows,

$$\tau_S = \sigma_n \tan \phi + c \quad [1]$$

where τ_S and σ_n are the shear and normal stresses (respectively) at the base of an arbitrary slice on the failure surface and ϕ , and c are the internal friction angle and cohesion of the ground (respectively).

In the problem considered in this study, the most common definition of *factor of safety* (FS) is adopted. This states that the factor of safety is the ratio of the shear strength of the ground on the failure surface and the shear stress required for equilibrium (see for example, Abramson et al. 2002; Coduto et al. 2011). Of the various formulations available for computing the factor of safety, the Bishop Method (as implemented in the software SLIDE) is employed in this study. The reader is referred to the widely available literature on slope stability analysis with limit equilibrium methods and the method of slices for more details about the implementation of the standard methods used in this study (see, for example, Duncan 1996; Abramson et al. 2002; Duncan et al. 2014; Huang 2014).

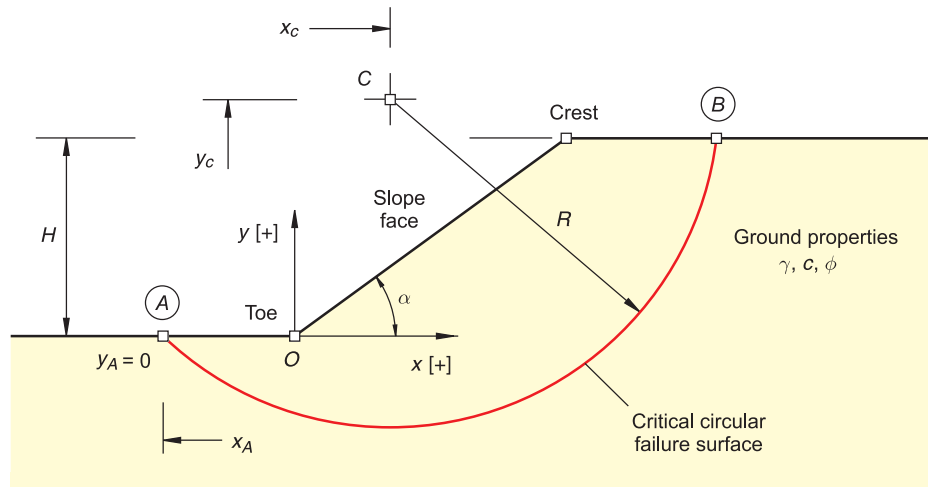


Figure 1. Slope excavated in *dry* ground assumed to obey the Mohr-Coulomb shear failure criterion.

3 Dimensionless representations of factor of safety and critical circular failure surface

For the slope introduced in Section 2 and following the analysis presented Hoek & Bray (1981), all three mechanical variables (γ , ϕ and c) and the single length-dimension variable (H) are conveniently grouped into a single dimensionless factor, referred to in this study as X , as follows

$$X = \frac{\gamma H \tan \phi}{c} \quad [2]$$

The advantage of using the dimensionless factor X is that the ratio of factor of safety and tangent of the internal friction angle depends on this ratio and the inclination angle of the slope (α) only, i.e.,

$$\frac{FS}{\tan \phi} = f_{FS}(X, \alpha) \quad [3]$$

In the equation above, f_{FS} is a function that can be 'traced' (i.e., reconstructed) by solving a series of selected slope cases for properly chosen values of the variables X and α , as will be explained later on in this section.

It is worth noting that equations [2] and [3] are the inverse of the dimensionless factors used by Hoek & Bray (1981). This is because this form permits a wider range of slopes to be studied, as also discussed in this section.

Additionally, all ratios of variables that characterize the position of the critical circular failure surface for the slope in Figure 1, depend on X and α only. For example, the *scaled* abscissa and ordinate of the center of the critical circular failure is defined as

$$\frac{x_c}{H} = f_{x_c}(X, \alpha) \quad [4]$$

and

$$\frac{y_c}{H} = f_{y_c}(X, \alpha) \quad [5]$$

The *scaled* abscissa and ordinate of the *starting* point of the critical circular failure surface (point A

in Figure 1) is defined as

$$\frac{x_A}{H} = f_{x_A}(X, \alpha) \quad [6]$$

and

$$\frac{y_A}{H} = f_{y_A}(X, \alpha) \quad [7]$$

As with the case of the function f_{FS} in equation [3], the functions f_{x_C} , f_{y_C} , f_{x_A} and f_{y_A} in equations [4] through [7] can also be reconstructed by solving a series of selected slope cases for properly chosen values of the variables X and α .

The scaled radius of the critical circular failure surface (R/H) can be also computed as the distance between the points C and A in Figure 1, i.e.,

$$\frac{R}{H} = \sqrt{\left(\frac{x_C}{H} - \frac{x_A}{H}\right)^2 + \left(\frac{y_C}{H} - \frac{y_A}{H}\right)^2} \quad [8]$$

As needed, the coordinates of the *ending* point B of the failure surface in Figure 1 can be determined as the intersection of the critical circular failure surface and the assumed horizontal plane on the crest of the slope.

It is worth noting that equations [4] through [8] have not been provided in Hoek & Bray (1981); these are included here to complete the representations originally proposed by those authors and to be able to define the position of the critical circular failure surface.

To reconstruct the functions of the dimensionless variables in equations [3] through [7], the limit equilibrium software SLIDE (Rocscience Inc. 2015) was employed. A total of 3,402 cases were evaluated using the Bishop method of slices implemented in the software. The input variables in the models were chosen so to obtain 81 equally spaced (in logarithm base-10 scale) slope cases of the factor X , given by equation [2], between 10^{-2} and 100. Slopes with slope face angles α between 20° and 80° with increments of 10° were chosen. The factors of safety and corresponding critical circular failure surfaces were determined for all cases using the 'Autorefine Search' option implemented in the software SLIDE. Appendix A provides a detailed discussion on the characteristics of the limit equilibrium models evaluated as part of this study.

To illustrate the reconstruction of these functions, Figure 2 shows the graphical representation of the function f_{FS} in equation [3], as obtained with SLIDE. The diagram defines the relationship between the scaled factor of safety $FS/\tan \phi$ (vertical axis) and the ratio X (horizontal axis) for different face slope angles α (the various curves in the diagram). The small dots on the curves represent the actual SLIDE cases that were evaluated. Moving towards the left side of the horizontal axis in Figure 2 (i.e., as X decreases), the ground is predominantly cohesive; moving towards the right side (i.e., as X increases), the ground is predominantly frictional. It can be shown that in the limit, when X tends to infinity, all different curves become asymptotic towards the scaled factor of safety predicted by the analytical solution of an infinite slope in purely frictional ground, i.e., $FS/\tan \phi = 1/\tan \alpha$ (see for example, Abramson et al. 2002; Coduto et al. 2011). Figure 2 shows the positive influence of the cohesion of the ground on factor of safety: for a fixed value of friction angle, the factor of safety increases significantly with the increase in cohesion. Figure 2 also shows the effect of the slope face angle on the factor of safety: for a fixed value of factor X , the factor of safety decreases with increase of the slope angle.

The results presented in Figure 2 were compared with the results summarized in the dimensionless chart for *dry* ground in Hoek & Bray (1981) and good agreement was found. In this regard it has to be noted that the dimensionless representations in Hoek & Bray (1981) allows proper readings of scaled factor of safety only for the range of the factor X from 0.25 to 100 —i.e., the representation in Figure 2, which considers a range of X from 0.01 to 100, extends further into the region where the

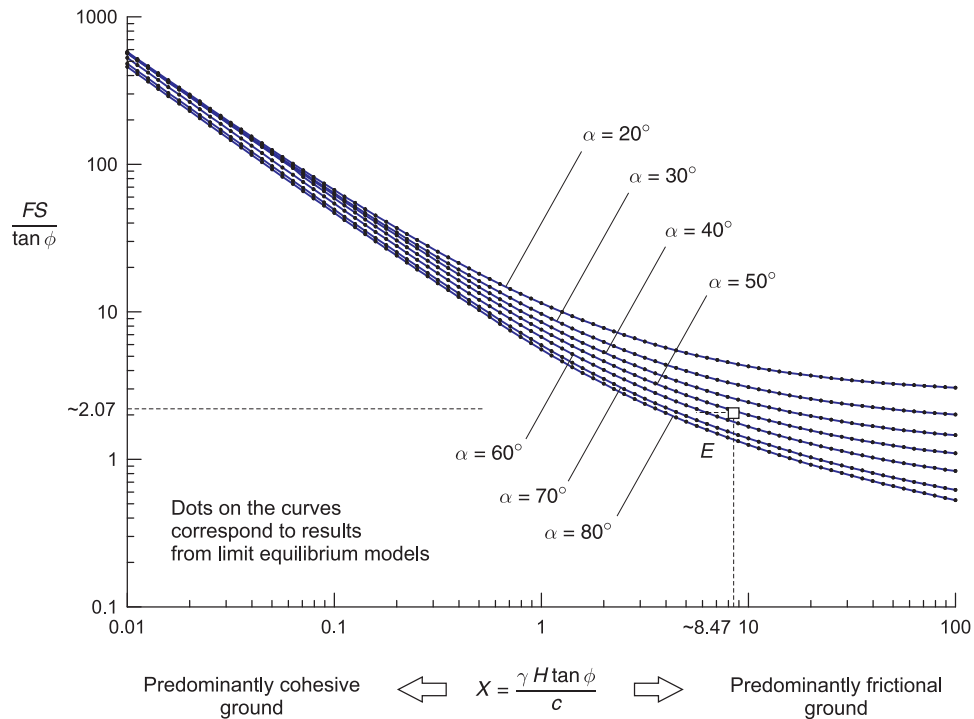


Figure 2. Dimensionless stability diagram for the estimation of the scaled factor of safety.

ground is predominantly cohesive.

A multiple regression analysis of the results represented in Figure 2 was carried out to obtain an algebraic equation to predict values of scaled factor of safety ($FS/\tan \phi$) as a function of the factor X and the angle α . The proposed equation and details of the regression analysis are presented in Appendix B.

For space reasons, no diagrams for the functions f_{x_c} , f_{y_c} , f_{x_A} and f_{y_A} in equations [4] through [7] are provided in this paper. Nevertheless, these diagrams can be easily constructed using the information provided in the EXCEL workbook, discussed later in Section 4.

To illustrate the application of the equations [3] through [7], the following case of slope geometry and ground properties is considered:

- Height of slope, $H = 300$ m
- Angle of slope, $\alpha = 52^\circ$
- Unit weight of the ground, $\gamma = 25$ kN/m³
- Internal friction angle of the ground, $\phi = 37^\circ$
- Cohesion of the ground, $c = 667$ kPa

For the given properties, the dimensionless variable $X = \gamma H \tan \phi / c$ results to be ~ 8.473 .

Using the values of functions f_{FS} , f_{x_c} , f_{y_c} , f_{x_A} and f_{y_A} in equations [3] through [7], as defined by the SLIDE models (and as computed by the logarithmic interpolation scheme implemented in the EXCEL workbook, discussed later on in Section 4), the following results are obtained:

- Scaled factor of safety, $FS/\tan \phi = 2.07$ ($FS = 1.56$ for $\phi = 37^\circ$); see Point *E* in Figure 2
- Scaled abscissa of the center of the critical failure surface, $x_c/H = -0.42$
($x_c = -126$ for $H = 300$ m)
- Scaled ordinate of the center of the critical failure surface, $y_c/H = 1.46$
($y_c = 438$ m for $H = 300$ m)
- Scaled abscissa of the *starting* point of the critical circular failure surface, $x_A/H = 0$
(note that the ordinate of the *starting* point of the critical failure surface is always zero)
- Scaled radius of the critical circular failure surface, $R/H = 1.52$
($R = 456$ m for $H = 300$ m)

The scaled factor of safety can also be estimated using the proposed equation presented in Appendix B (see equations [B-1] and [B-3]). This gives $FS/\tan \phi = 2.03$ ($FS = 1.53$ for $\phi = 37^\circ$), which implies there is a negative error of $\sim 2\%$, if the solution obtained with the dimensionless representations (which is derived from SLIDE models) is assumed to be the correct one (see Appendix B for more details).

Another important aspect of the functions of the dimensionless variables in equations [3] through [7] is that they allow to reveal the nature of mechanical similarity of stability conditions for slopes, particularly the similarity of scaled factors of safety and location of critical circular failure surface.

To illustrate the concept, Figure 3 includes a diagram similar to the one represented in Figure 2 but considering only three curves corresponding to slope angles equal to 30° , 50° and 70° . The six slope sketches included in the diagram show the corresponding failure surfaces defined from equations [4] through [8] (with the EXCEL workbook discussed in Section 4) for the three slope inclination angles and for arbitrarily selected cases of the factor X equal to 0.05, 1 and 25. Figure 3 confirms the known fact that the critical circular failure surface is deeper for predominantly cohesive ground and shallower for predominantly frictional ground. The diagram defines the scaled factor of safety and shape of the critical circular failure surface for slopes characterized by particular values of X and α .

The concept of similarity is further illustrated by the following analysis. Table 1 lists the cases of five slopes with the same inclination angle but otherwise significantly different values of slope height, ground unit weight, friction angle and cohesion. The Case 4 in the table corresponds to the same example described above for which the height of the slope is 300 m (note that Cases 1 and 5 in the table, which correspond to slopes of unrealistic heights, are included for illustration purposes only).

The five different cases listed in Table 1 are characterized by the same values of similarity constants X and α , and therefore by the same values of the functions ' f ' in equations [3] through [7]. Because of this, and as shown in Figure 4, all five cases will have the same values of scaled factor of safety and scaled coordinates that define the position of the critical circular failure surface. Therefore, the cases can be said to be *mechanically similar* with regard to stability conditions.

Table 1. Example of slopes displaying mechanical similarity of factor of safety and critical failure surface location.

Case	α [°]	H [m]	γ [kN/m ³]	ϕ [°]	c [kPa]	$X = \gamma H \tan \phi / c$ [-]
1	52	0.3	25	45	8.852×10^{-1}	8.473
2		3	19	15	1.803	
3		30	24	35	5.95×10^1	
4		300	25	37	6.67×10^2	
5		3,000	27	8	1.344×10^3	

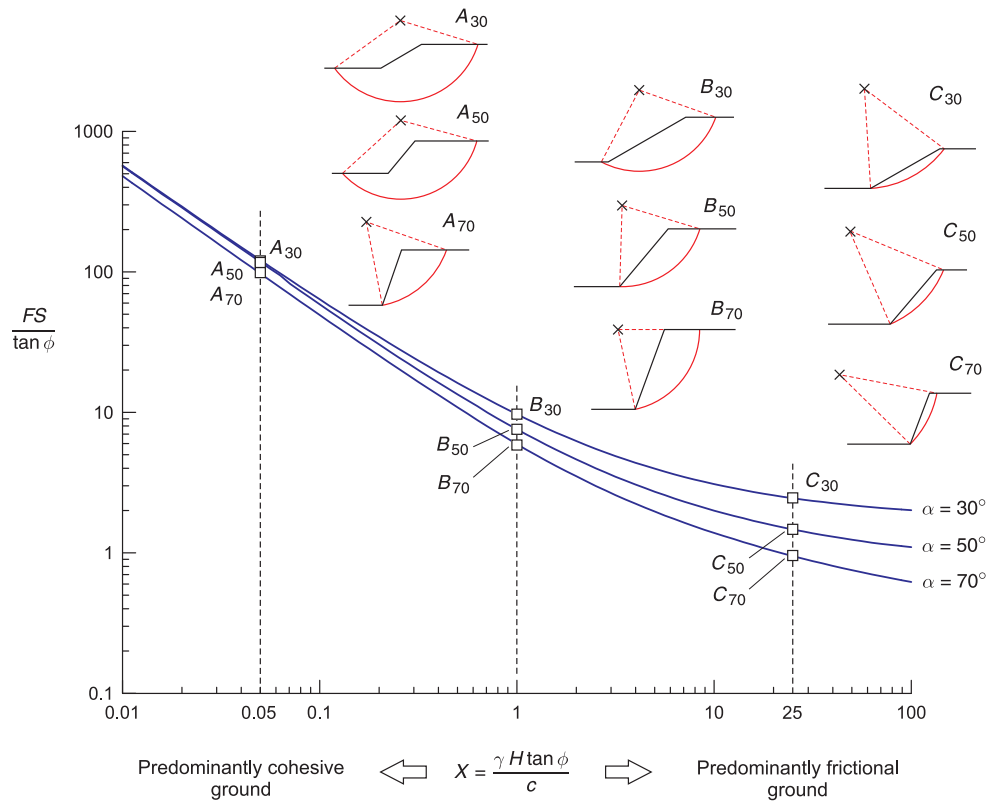


Figure 3. Dimensionless stability diagram showing similarity of scaled factor of safety and critical failure surface location.

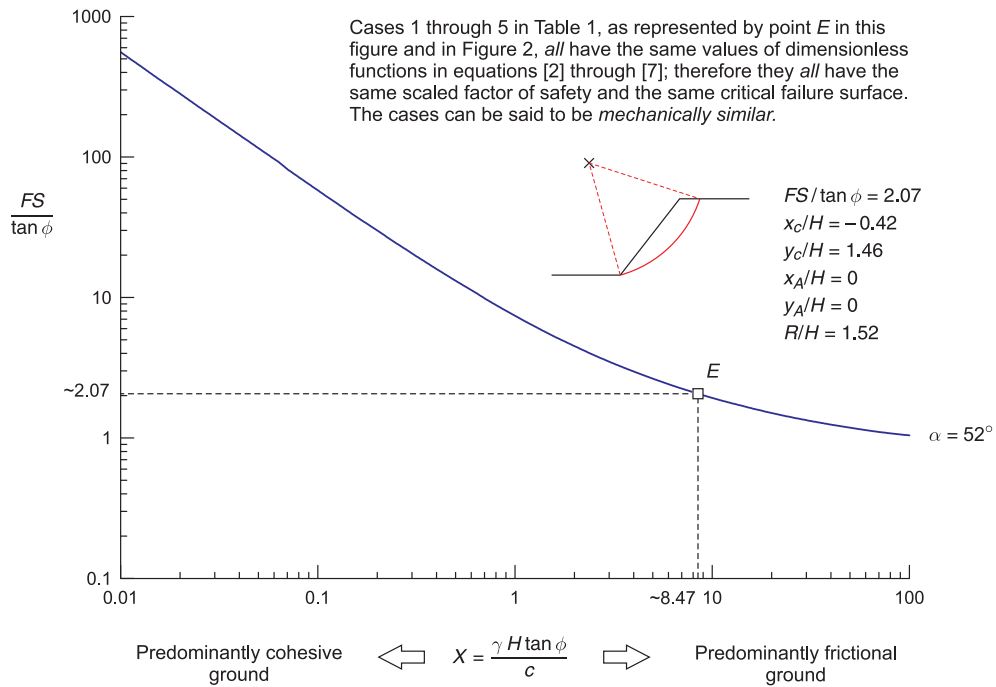


Figure 4. Dimensionless stability diagram showing similarity of the factor of safety and critical failure surface location for the slope cases in Table 1.

4 Computer implementation of the dimensionless stability representations

Although dimensionless graphical representations or *dimensionless charts* as discussed in the previous sections have been the traditional means of summarizing and sharing results of procedures for obtaining stability results by various authors, in modern geotechnical design practice, engineers typically prefer the use of computer spreadsheets over the use of these graphical dimensionless representations (Hoek 2000).

With this idea in mind, another computational tool provided in this paper (supplementary to the diagrams introduced in Section 3 and the equations provided in Appendix B) is an EXCEL (Microsoft 2016) workbook called 'Slope Stability Calculator for Mohr-Coulomb Dry Ground'.

This EXCEL workbook contains the tabulated values of the functions f_{FS} , f_{Xc} , f_{Yc} , f_{XA} and f_{YA} in equations [3] through [7] as obtained with the software SLIDE (see Appendix A for details) and implements a polynomial interpolation scheme that allows the user to obtain values of factor of safety and location of the circular critical failure surface for any slope (with resulting factors X and angles α falling in the ranges discussed in the previous section).

The main worksheet in this EXCEL workbook is shown in Figure 5. The user defines the geometry of the slope and the properties of the ground in the section entitled 'Input Data'. Results are displayed in the section 'Results'. If specified in the input data in the main worksheet, another worksheet presents a basic plot of the properly scaled slope, showing the position of the critical circular failure surface and a list of input data and results. Figure 6 shows a view of the worksheet with the graphical representation of the problem, including the summary of input data and results.

Note that the particular input values and results displayed in Figures 5 and 6 correspond to the very same slope case discussed in Section 3.

The EXCEL file corresponding to the workbook presented in this section can be freely downloaded from the first author's web site at www.d.umn.edu/~carranza/SLOPE18.

Note that although computation of results is implemented through formulas without the use of macros, the EXCEL workbook uses a VBA (Visual Basic for Applications) macro for constructing the scaled plot of the slope problem (if asked by EXCEL, the user should allow EXCEL to activate the macro in order for the plot to be generated).

5 Practical application example

Figure 7 shows a view of a slope in a sector of an open pit mine in Chile that was analyzed using the proposed method. The slope has 10 double-benches with a bench height of 30 m and a bench width of approximately 13 m. The bench face angle is 68° . This results in a total slope height, $H = 300$ m, and an overall slope angle (measured from toe to crest), $\alpha = 52^\circ$. For the open pit slope shown in Figure 7, at the scale of the full height of the slope, the joint spacing is small enough relative to the slope height that the assumption of ground continuity and isotropy can be considered valid (Read & Stacey 2009; Wyllie 2018).

The rock mass is characterized by the following Hoek-Brown properties:

- Geological Strength Index, $GSI = 50$
- Disturbance Factor, $D = 0.7$
- Unconfined Compressive Strength (intact rock), $\sigma_{ci} = 50$ MPa
- Hoek-Brown constant, $m_i = 12$

The rock mass is assumed to have an average unit weight, $\gamma = 25$ kN/m³.

Using the procedure described in Hoek et al. (2002), considering an interval of minor principal stresses in the range 0 to 2.5 MPa, the Mohr-Coulomb internal friction angle and cohesion were estimated to be $\phi = 37^\circ$ and $c = 667$ kPa, respectively.

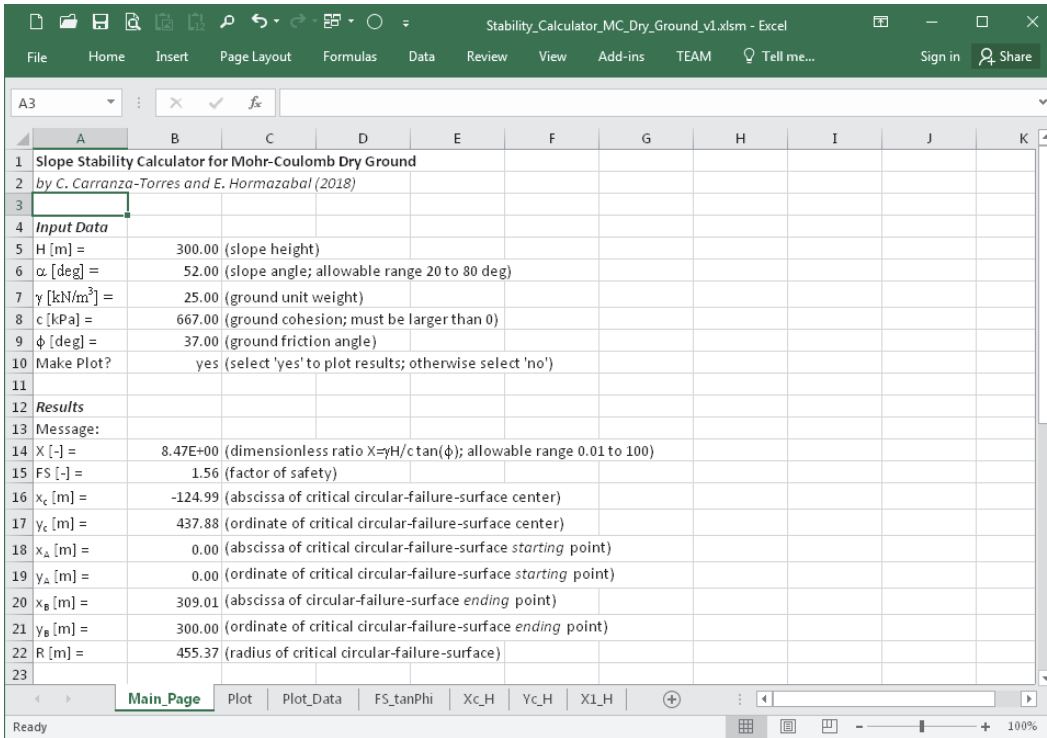


Figure 5. View of the main worksheet in the EXCEL workbook for implementation of stability computations.

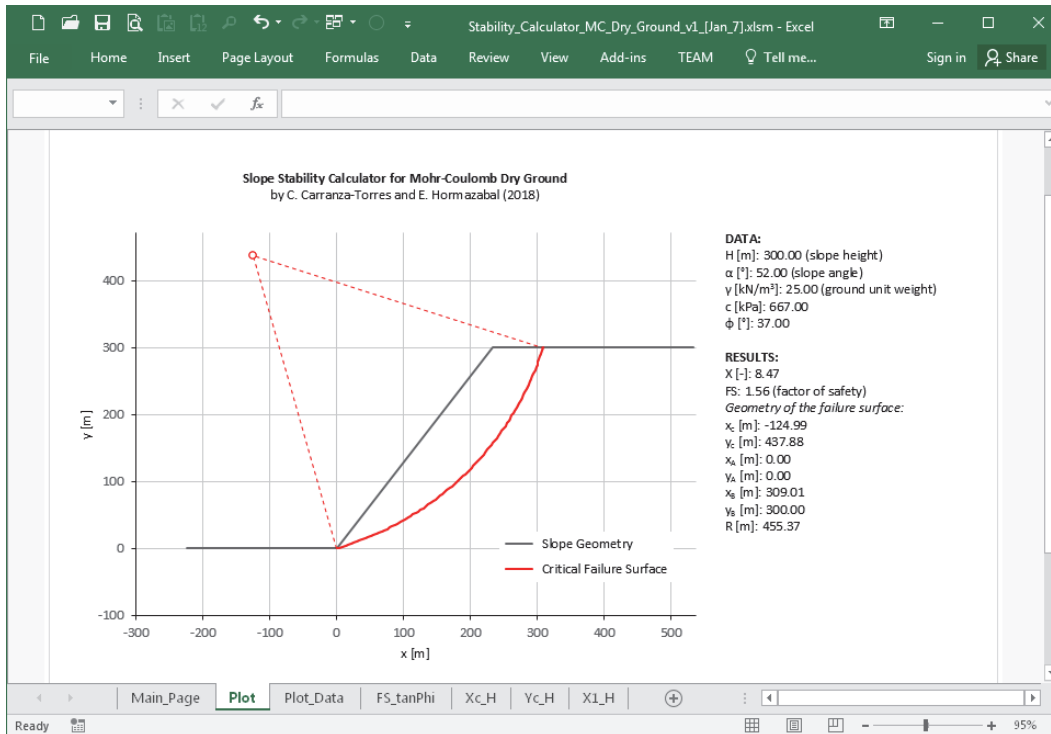


Figure 6. View of the worksheet showing the graphical representation of the slope problem in the EXCEL workbook for implementation of stability computations.

As it can be seen, this slope problem corresponds to the very same slope case discussed already in Section 3 (see point *E* in Figure 2; see also Case 4 in Table 1, and Figure 4) and in Section 4 (see Figures 5 and 6).

The factor of safety for the slope and the critical circular failure surface were already estimated to be as follows (see, for example, Figures 5 and 6):

- Factor of safety, $FS = 1.56$
- Abscissa of the center of the critical circular failure surface, $x_C = -124.99$ m
- Coordinate of the center of the critical circular failure surface, $y_C = 437.88$ m
- Radius of the critical circular failure surface, $R = 455.37$ m

To confirm the validity of these results, a section of the slope shown in Figure 7 was solved with the software SLIDE (Rocscience Inc. 2015), in one instance considering the slope face with the actual benches, and in the other instance considering a planar face linking the toe and the crest of the actual slope. Figure 8 shows a view of the results obtained with the software SLIDE for the first case in which benches are considered. The figure includes the different circular failure surfaces analyzed by the software, using the same procedure for locating the critical circular failure surface described in Appendix A. Figure 8 also shows the critical circular failure surface corresponding to the minimum factor of safety for the slope —this is indicated with a thick continuum line in Figure 8. The factor of safety obtained with the software is $1.572 \sim 1.57$ which is approximately equal to the one obtained with the proposed method (i.e., 1.56). Figure 8 also includes the location of the critical failure surface obtained with the proposed method (as discussed in the example in Section 3) and with SLIDE, when the same slope case was solved with SLIDE but with a planar slope face —this is indicated with a dashed line in Figure 8. The location of the critical failure surfaces in both instances is practically the same.



Figure 7. View of a benched slope in an open pit mine used to illustrate the application of the proposed stability analysis tools.

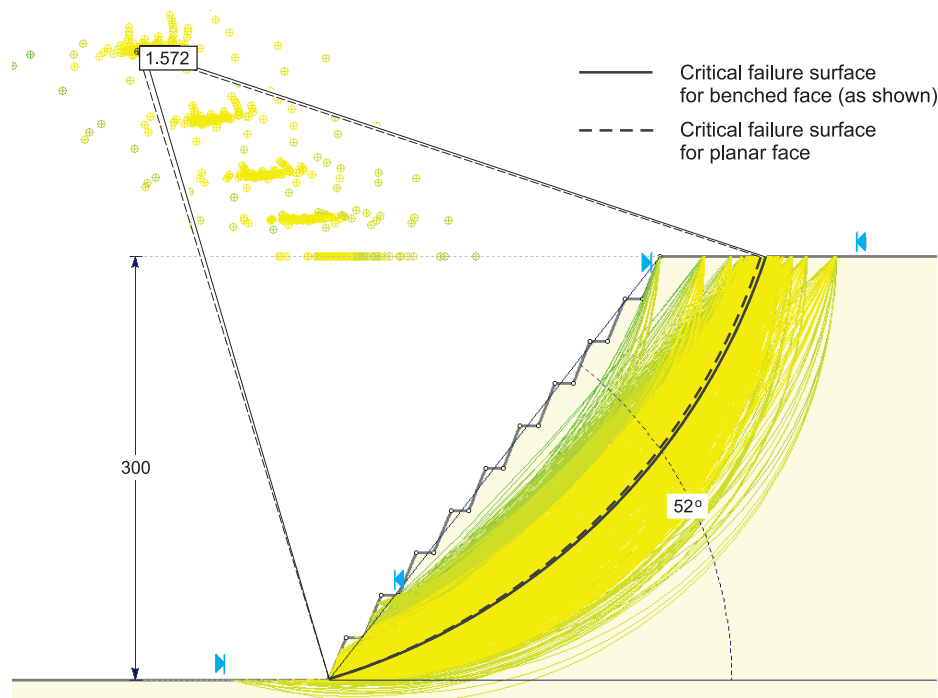


Figure 8. View of the SLIDE (Rocscience Inc. 2015) analysis of a section of the benched slope in Figure 7.

6 Discussion

The tools presented in this paper, including graphical representations, equations and computer EXCEL workbook, can be used to make a quick determination of factor of safety and critical circular failure surface location for slopes excavated in Mohr-Coulomb *dry* ground. The application of these tools could be particularly useful in the stage of pre-design of projects involving slopes, when different slope angles or heights, or different ground properties need to be evaluated.

It needs to be emphasized that the adoption of the *limit equilibrium* method and the Bishop formulation, in particular, used to develop the tools presented in this paper was due to efficiency reasons only —i.e., to be able to generate thousands of models and obtain results in the fastest way possible. Similar representations could have been developed with the *limit analysis* or *shear strength reduction* methods discussed in Section 1 —although in the last case, an unreasonable amount of time would have been required to process all models needed to develop these tools. It is important to remark that for the simple slope cases addressed in this paper (i.e., slopes with planar face in homogeneous/isotropic frictional-cohesive material) no significant differences in values of factor of safety or location of the critical failure surface could be expected when applying *limit equilibrium*, *limit analysis* or *shear strength reduction* methods (see, for example, Baker 1980; Yu et al. 1998; Dawson et al. 1999; Cheng et al. 2007; Leshchinsky 2013). In any case, due to the non-existence of a rigorous closed-form solution for the problem of computing the factor of safety and location of the critical failure surface, all of the methods available to carry out stability analyses of the slopes addressed in this paper (i.e., *limit equilibrium*, *limit analysis* and *strength reduction technique*) will be expected to give an *approximate* solution to the problem only.

Because the results obtained with the proposed tools are approximate in nature, caution must be exercised when applying these tools. In the context of using the *limit equilibrium* method as done in this paper, the approximate nature of the results can be further explained by the fact that slightly different values of factor of safety and/or slightly different failure surface locations could result from

application of limit equilibrium (SLIDE) models if they are re-evaluated with other methods of factor of safety evaluation (e.g., different from the Bishop method), or different critical search method (e.g., other than the 'Autorefine Search' method) or with some other different features (e.g., number of slices different from 50, no implicit inclusion of a tensile crack at the crest of the slope and others). In every case, when the tools are applied in the pre-design stage, it is recommended to always carry out further validation of the stability conditions with other methods, including other stability analysis methods and empirical methods.

The analysis presented in this paper could be extended further to account for other ground conditions. One of these conditions is the case in which the ground is purely cohesive (the internal friction angle is zero). For this case, due to the occurrence of the internal friction angle of the ground in the denominator of equation [3], computation of factors of safety and location of the critical circular failure surface will not be possible (it would still be possible to obtain results if a relatively small value of internal friction angle is used in the computational tools presented in this paper, although the results will be prone to numerical errors). Particular dimensionless representations that account for purely cohesive ground conditions could be developed.

Another condition of interest and of practical importance is that of water presence in the ground. Hoek & Bray (1981) presented dimensionless representations for five different cases of phreatic surface behind the slope face. The analysis presented in this paper could be extended to those cases as well, and similar tools as introduced here could be developed to account for the presence of water in the ground.

7 Acknowledgements

The authors would like to thank Dr. Evert Hoek for the critical review and recommendations for improvement provided during development of the first draft version of this paper. The authors would also like to express their gratitude to Mr. Felipe Sanz Lizt at SRK Consulting Chile, for assistance with the development of the Excel worksheet presented in Section 4 of this paper.

References

- Abramson, L. W., Lee, T. S., Sharma, S., M., G. & Boyce 2002. *Slope stability and stabilization methods* (2nd ed.). John Wiley & Sons. New York.
- Baker, R. 1980. Determination of the critical slip surface in slope stability computations. *International Journal for Numerical and Analytical Methods in Geomechanics* 4(4), 333–359.
- Baker, R. 2003. A second look at Taylor's stability chart. *Journal of Geotechnical and Geoenvironmental Engineering* 129(12), 1102–1108.
- Bell, J. M. 1966. Dimensionless parameters for homogeneous earth slopes. *Journal of Soil Mechanics & Foundations Div. ASCE SM* 5(GT9), 51–65.
- Bishop, A. W. 1955. The use of the slip circle in the stability analysis of slopes. *Géotechnique* 5(1), 7–17.
- Bishop, A. W. & Morgenstern, N. R. 1960. Stability coefficients for earth slopes. *Géotechnique* 10(1), 129–150.
- Chapra, S. C. & Canale, R. P. 2015. *Numerical methods for engineers* (7th ed.). Mc Graw Hill. New York.
- Cheng, Y. M., Lansivaara, T. & Wei, W. B. 2007. Two-dimensional slope stability analysis by limit equilibrium and strength reduction methods. *Computers and Geotechnics* 34(3), 137–150.
- Coduto, D. P., Yeung, M. C. & Kitch, W. A. 2011. *Geotechnical engineering. Principles and practices* (2nd ed.). Pearson.
- Cousins, B. F. 1978. Stability charts for simple earth slopes. *Journal of the Geotechnical Engineering Division* 104(2), 267–279.
- Dawson, E. M., Roth, W. H. & Drescher, A. 1999. Slope stability analysis by strength reduction. *Geotechnique* 49(6), 835–840.
- Duncan, J. M. 1996. State of the art: limit equilibrium and finite-element analysis of slopes. *Journal of Geotechnical Engineering* 122(7), 577–596.

- Duncan, J. M., Wright, S. G. & Brandon, T. L. 2014. *Soil Strength and Slope Stability*. John Wiley & Sons.
- Fine Inc. 2016. *GEO5. Slope stability analysis software based on the limit equilibrium method*. Praha, Czech Republic.
- Geo-Slope Inc. 2012. *SLOPE/W Version 2012. Slope stability analysis software based on the limit equilibrium method*. Calgary, Canada.
- Griffiths, D. V. & Lane, P. A. 1999. Slope stability analysis by finite elements. *Geotechnique* 49(3), 387–403.
- Haines, A., Terbrugge, P. J., Carrieri, P. J. & Others 1991. Preliminary estimation of rock slope stability using rock mass classification systems. In *7th ISRM Congress*. International Society for Rock Mechanics (ISRM).
- Hammah, R. E., Yacoub, T. E. & Curran, J. H. 2007. Serviceability-based slope factor of safety using the shear strength reduction (SSR) method. In L. R. e Sousa, C. Olalla, & N. Grossmann (Eds.), *Proceedings of the 11th Congress of the International Society for Rock Mechanics*, Lisbon.
- Hoek, E. 2000. Personal communication.
- Hoek, E. & Bray, J. 1981. *Rock slope engineering* (3rd ed.). CRC Press. London.
- Hoek, E. & Brown, E. T. 1980. Empirical strength criterion for rock masses. *J. Geotech. Eng. Div. ASCE* 106(GT9), 1013–1035.
- Hoek, E. & Brown, E. T. 1997. Practical estimates of rock mass strength. *International Journal of Rock Mechanics and Mining Sciences* 34(8), 1165–1186.
- Hoek, E., Carranza-Torres, C. & Corkum, B. 2002. Hoek-Brown failure criterion – 2002 edition. In *Proceedings of NARMS-TAC 2002, Mining Innovation and Technology. Toronto – 10 July 2002*, pp. 267–273. University of Toronto. (Available for downloading at Hoek's Corner, www.rocscience.com).
- Huang, Y. H. 2014. *Slope stability analysis by the limit equilibrium method. Fundamentals and methods*. American Society of Civil Engineers (ASCE) Press. Reston, Virginia.
- Interactive Software Designs Inc. 2007. *XSTABL. Slope stability analysis software based on the limit equilibrium method*. Moscow, Idaho.
- Janbu, N. 1954a. Application of composite slip surfaces for stability analysis. In *European Conference on Stability of Earth Slopes. Stockholm, Sweden*, Volume 3, pp. 43–49.
- Janbu, N. 1954b. *Stability analysis of slopes with dimensionless parameters*. Thesis for the Doctor of Science in the Field of Civil Engineering. Harvard University, Soil Mechanics Series, No. 46.
- Juang, C. H., Jhi, Y. Y. & Lee, D. H. 1998. Stability analysis of existing slopes considering uncertainty. *Engineering Geology* 49(2), 111–122.
- Kotze, G. & Bosman, J. 2015. Towards expediting large-scale slope design using a re-worked design chart as derived from limit equilibrium methods. In *In Slope Stability 2015: International Symposium on slope stability in open pit mining and civil engineering.*, pp. 341–362. Cape Town Convention Centre, Cape Town, 12–14 October 2015. Johannesburg: The Southern African Institute of Mining and Metallurgy.
- Leshchinsky, B. 2013. Comparison of limit equilibrium and limit analysis for complex slopes. In *Geo-Congress 2013: Stability and Performance of Slopes and Embankments III*, pp. 1280–1289.
- Matsui, T. & San, K. C. 1992. Finite element slope stability analysis by shear strength reduction technique. *Soils and foundations* 32(1), 59–70.
- Michalowski, R. L. 2002. Stability charts for uniform slopes. *Journal of Geotechnical and Geoenvironmental Engineering. ASCE* 128-4(GT9), 351–355.
- Microsoft 2016. *Excel Software. Version 2016*. Microsoft. Redmond, Washington.
- Morgenstern, N. R. & Price, V. E. 1965. The analysis of the stability of general slip surfaces. *Géotechnique* 15(1), 77–93.
- O'Connor, M. J. & Mitchell, R. J. 1977. An extension of the Bishop and Morgenstern slope stability charts. *Canadian Geotechnical Journal* 14(1), 144–151.
- Potts, D. M. & Zdravkovic, L. 1999. *Finite element analysis in geotechnical engineering. Theory*. Thomas Telford. London: Thomas Telford.
- Read, J. & Stacey, P. 2009. *Guidelines for open pit slope design*. CSIRO Publishing. Melbourne, Australia.
- Rocscience Inc. 2015. *SLIDE Version 7. Slope stability analysis software based on the limit equilibrium method*. Toronto, Canada.
- Sjoberg, J. 2000. Failure mechanisms for high slopes in hard rock. In W. A. Hustrulid, M. K. McCarter, & D. J. A. V. Zyl (Eds.), *Slope Stability in Surface Mining*, pp. 71–80. Society for Mining, Metallurgical and Exploration (SME). Littleton, Colorado.
- Spencer, E. 1967. A method of analysis of the stability of embankments assuming parallel inter-slice forces. *Géotechnique* 17, 11–26.
- Steffen, O. K. H., Contreras, L. F., Terbrugge, P. J. & Others 2008. A risk evaluation approach for pit slope design. In *The 42nd US Rock Mechanics Symposium (USRMS)*. American Rock Mechanics Association (ARMA).

- Steward, T., Sivakugan, N., Shukla, S. K. & Das, B. M. 2010. Taylor's slope stability charts revisited. *International Journal of Geomechanics* 11(4), 348–352.
- Taylor, D. W. 1948. *Fundamentals of Soil Mechanics*. Wiley. New York.
- Vanmarcke, E. H. 1980. Probabilistic stability analysis of earth slopes. *Engineering Geology* 16(1-2), 29–50.
- Verruijt, A. 2012. *Soil Mechanics*. Delft University of Technology, Delft, The Netherlands (Available for free downloading at <http://geo.verruijt.net/>).
- Wyllie, D. C. 2018. *Rock slope engineering. Civil Applications*. CRC Press. Taylor & Francis.
- Yu, H. S., Salgado, R., Sloan, S. W. & Kim, J. M. 1998. Limit analysis versus limit equilibrium for slope stability. *Journal of Geotechnical and Geoenvironmental Engineering* 124(1), 1–11.

Appendix A. Characteristics of the limit equilibrium models used to define the dimensionless graphical representations

This appendix provides details on the 3,402 slope cases solved with the software SLIDE (Rocscience Inc. 2015), used to produce the dimensionless graphical representations and the EXCEL workbook presented in the main text.

For most practical problems, the range of values of the variable X (see equation [2]) was determined to be in the interval 10^{-2} to 100. This range was determined by application of a Monte-Carlo simulation that evaluated the variable X for thousands of non-correlated random values generated from a uniform distribution with the following ranges of slope height and ground properties:

- Slope height, $H = 1$ m to 500 m
- Unit weight of the ground, $\gamma = 15$ kN/m³ to 27 kN/m³
- Internal friction angle of the ground, $\phi = 5^\circ$ to 75°
- Cohesion of the ground, $c = 100$ kPa to 500 kPa

Seven different cases of slope inclination angle ranging from 20° to 80° , in increments of 10° , were considered (vertical slopes were not considered, as they led to very thin critical failure surfaces, particularly, for predominantly frictional ground).

For each slope face angle, a total number of 81 slope cases for values of X equally spaced (when plotted in logarithm base-10 scale) in the range 10^{-2} to 100 were first evaluated. For each of these cases, the slope height and ground properties were obtained randomly, from the range of values listed above. The computation of factor of safety and location of the critical failure surface was repeated three times (for three different combinations of random input values) to check consistency in the results, bringing the total number of cases analyzed with SLIDE to 1,701 (i.e., $7 \times 81 \times 3$). The search process of the critical failure surface in SLIDE was implemented in two stages (i.e., each model was solved twice), as explained later on in this appendix, thus bringing the grand total number of cases analyzed with SLIDE to 3,402.

Each SLIDE model was constructed using the following geometrical characteristics: denoting the length of the slope face as L , the left and right boundaries of the slope model were both located at a horizontal distance of $5L$ from the toe and crest of the slope, respectively; the lower boundary of the model was located at a vertical distance of $2.5L$ from the toe of the slope.

The factor of safety was computed using the Bishop method implemented in SLIDE, assuming 50 slices above the failure surface, and a factor of safety tolerance of 0.005 (with a maximum of 75 iterations) in the iterative implementation of the method.

The search process of the critical circular failure surface was done using the 'Autorefine Search' option implemented in the software SLIDE (the documentation of the software states that this method is the most efficient search method available in the software), using default input parameters (i.e., divisions along slope, circles per division, and number of iterations, all equal to 10; divisions in next iteration equal 50%). As mentioned above, the search process was performed in two stages. In

the first stage, the 'Autorefine Search' option was applied to the full upper surface of the model. In the second stage, the search was limited to intervals for the *starting* and *ending* points of the failure surface (see points *A* and *B*, respectively in Figure 1), centered around the *starting* and *ending* points for the critical failure surface obtained in the first stage; in this more localized search, the search intervals for *starting* and *ending* points of the failure surface both had a length of 50% the length of the face of the slope (as an example, Figure 8 shows the second stage of searching of the critical failure surface; note that the length of the search segments defined by the 'triangular' marks near the toe and crest of the slope is 50% the length of the face of the slope).

The results from all models solved with SLIDE were finally scaled according to equations [3] through [8], and incorporated into the EXCEL workbook discussed in Section 4.

Appendix B. Proposed equation to compute factor of safety of slopes in Mohr-Coulomb dry ground

A multiple regression analysis of the results represented in Figure 2 was carried out to obtain an algebraic equation to predict values of scaled factor of safety ($FS/\tan \phi$) as a function of the factor X and the angle α . With this purpose the method of minimization of the sum of square of the estimate residuals was used (Chapra & Canale 2015). The fitting equation is an inverse power equation of the following form:

$$\frac{FS}{\tan \phi} = \frac{1}{\tan \alpha} + \frac{g_1(\alpha)}{X} + \frac{g_2(\alpha)}{X^{g_3(\alpha)}} \quad [\text{B-1}]$$

where the functions $g_1(\alpha)$, $g_2(\alpha)$ and $g_3(\alpha)$ are cubic polynomials that show a discontinuity of the first and higher derivatives at $\alpha = 50^\circ$ (the approximate value of slope angle above which the critical circular failure surface will always have a *starting* point that coincides with the toe of the slope —see point *A* in Figure 1).

These functions are defined as follows:

If $\alpha \leq 50^\circ$

$$\begin{aligned} g_1(\alpha) &= 5.523 - 1.032 \times 10^{-2} (\alpha - 50) - 1.396 \times 10^{-3} (\alpha - 50)^2 - 2.748 \times 10^{-5} (\alpha - 50)^3 \\ g_2(\alpha) &= 1.346 - 4.899 \times 10^{-2} (\alpha - 50) + 8.010 \times 10^{-4} (\alpha - 50)^2 + 6.834 \times 10^{-6} (\alpha - 50)^3 \\ g_3(\alpha) &= 3.755 \times 10^{-1} - 9.464 \times 10^{-3} (\alpha - 50) - 1.307 \times 10^{-4} (\alpha - 50)^2 + 4.509 \times 10^{-7} (\alpha - 50)^3 \end{aligned} \quad [\text{B-2}]$$

If $\alpha \geq 50^\circ$

$$\begin{aligned} g_1(\alpha) &= 5.523 - 3.486 \times 10^{-2} (\alpha - 50) - 1.186 \times 10^{-3} (\alpha - 50)^2 + 3.900 \times 10^{-5} (\alpha - 50)^3 \\ g_2(\alpha) &= 1.346 - 8.101 \times 10^{-3} (\alpha - 50) - 6.782 \times 10^{-4} (\alpha - 50)^2 + 2.197 \times 10^{-5} (\alpha - 50)^3 \\ g_3(\alpha) &= 3.755 \times 10^{-1} - 2.914 \times 10^{-3} (\alpha - 50) + 1.276 \times 10^{-4} (\alpha - 50)^2 - 5.405 \times 10^{-6} (\alpha - 50)^3 \end{aligned} \quad [\text{B-3}]$$

It has to be emphasized that the regression analysis was done considering that the slope inclination angle α in the equations above is expressed in degrees and not in radians (e.g., when using these equations to compute the scaled factor of safety of slope with inclination angle 45° , the equations must consider the variable α to be 45 and not $\pi/4$).

With regard to equation [B-1], the reason for choosing the particular form of an inverse power equation is to be able to recover the solution of an infinite slope when the ground is purely frictional —i.e., $FS/\tan \phi = 1/\tan \alpha$ when $X \rightarrow \infty$ (see for example, Abramson et al. 2002; Coduto et al. 2011).

As with any regression analysis, application of equations [B-1] through [B-3] to compute the scaled factor of safety can be expected to show some error with respect to the original results obtained with the limit equilibrium models; this error is an intrinsic consequence of the fitting process.

The remainder of this appendix presents a discussion on the expected error of the equations [B-1] through [B-3] and shows that these equations can either overestimate or underestimate the scaled

factor of safety within a margin of approximately $\pm 5\%$.

Figure B-1 shows a similar representation as in Figure 2, but obtained with the proposed equations. At first sight, the diagrams in Figure B-1 and Figure 2 are identical. Nevertheless, because equations [B-1] through [B-3] are best fit equations obtained from polynomial regression analysis, there will be some error associated with the estimation of scaled factor of safety.

To quantify this error, the dimensionless representation of scaled factor of safety of SLIDE models given by equation [3] (with the function f_{FS} as shown in Figure 2) can be considered to be the true solution of the problem. In such case, the absolute error can be computed as follows

$$\frac{FS}{\tan \phi} \text{ Error [\%]} = \frac{FS/\tan \phi \text{ (with Eq. [3])} - FS/\tan \phi \text{ (with Eq. [B-1])}}{FS/\tan \phi \text{ (with Eq. [3])}} \tag{B-4}$$

Figure B-2 is the graphical representation of equation [B-4]. The figure suggests that the error associated with application of equations [B-1] through [B-3] can be positive or negative (i.e., the scaled factors of safety can be either overestimated or underestimated, respectively), and that for all cases of the stability factor X considered in this study, the absolute value of the error is not larger than approximately 5%. The authors recommend caution when applying the equations [B-1] through [B-3], because there is a certain degree of error associated with the (function) fitting process; also, and as discussed in Section 6, the dimensionless limit equilibrium results from which these equations have been derived, are understood to be approximate in nature.

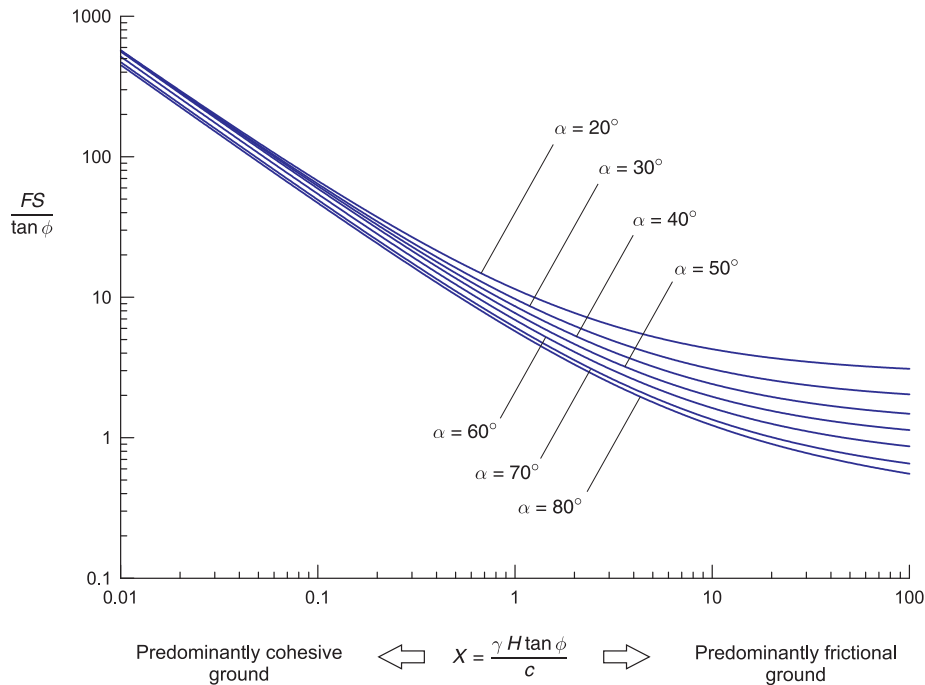


Figure B-1. Dimensionless stability diagram for the estimation of the scaled factor of safety obtained with equations [B-1] through [B-3].

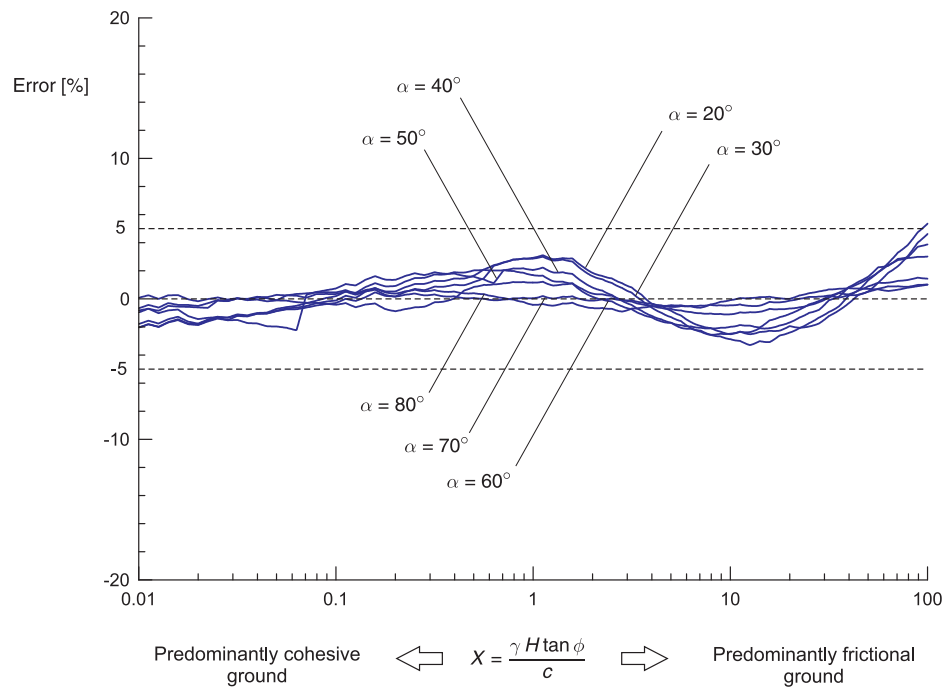


Figure B-2. Graphical representation of scaled factor of safety error computed with equation [B-4].